EAI Endorsed Transactions
on Energy Web
Research Article EAI.EU

Partial Discharge Detection and Identification in High-Voltage Cable Systems Based on Heterogeneous Sensor Fusion and Enhanced Deep Learning

Ling Gao*, Lixing Zhang, Qi Hu, Lining Jia, Xue Zhao, Penglong Liu, Bozhi Liu, Shunjin Shi

State Grid Jibei Electric Power Co., Ltd., Tangshan Power Supply Company, Tangshan 063000, China

Abstract

High-voltage cable systems are critical components of power transmission networks, where partial discharge (PD) can cause insulation degradation and severe operational failures. Accurate detection and reliable identification of PD are therefore essential, yet conventional methods are often vulnerable to electromagnetic interference and exhibit limited recognition performance. This paper proposes a PD detection and identification framework for high-voltage cable systems based on heterogeneous sensor fusion and enhanced deep learning. A high-speed optical electric-field sensor is employed to localize potential insulation defects, while an acoustic pressure wave sensor is used to confirm PD occurrence and intensity. An improved adaptive-threshold discrete wavelet transform is applied for signal denoising, and an optimized Gramian Angular Field transformation converts one-dimensional signals into two-dimensional feature representations. A residual convolutional neural network incorporating an efficient channel attention mechanism is then developed for PD pattern identification. Experiments involving corona, void, and surface discharges demonstrate that the proposed system achieves a 100% PD detection rate and a recognition accuracy of 96.0% under laboratory conditions. Field tests on 220 kV tunnel-laid cables further verify that both detection and identification accuracies reach 100%, with superior robustness and environmental adaptability compared with conventional approaches.

Keywords: Partial discharge, High-voltage cable systems, Heterogeneous sensor fusion, Deep learning, Pattern identification, Condition monitoring.

Received on 08 September 2025, accepted on 20 December 2025, published on 04 May 2026

doi: 10.4108/ew.12824

1. Introduction

High-voltage cable systems play a vital role in modern power transmission networks, especially in urban power grids and underground infrastructures where compact layout and high reliability are required [1,2]. However, long-term exposure to complex operating conditions, such as thermal stress, electrical stress, mechanical vibration, and environmental factors, can lead to insulation deterioration. Partial discharge (PD), as a typical manifestation of insulation defects, is widely recognized as a key precursor to insulation failure and catastrophic power system accidents. Therefore, accurate detection and reliable identification of PD activities are essential for condition monitoring and preventive maintenance of high-voltage cable systems [3].

Conventional PD detection techniques mainly rely on single-modality electrical measurements, including ultra-high-frequency (UHF) sensing, pulse current methods, and high-frequency current transformers [4-6]. Although these approaches have been extensively applied in laboratory and field environments, their performance is often degraded by strong electromagnetic interference, background noise, and complex installation conditions in practical engineering scenarios. Moreover, single-sensor-based methods usually provide limited information about PD characteristics, making

* Corresponding author. Email: 849988415@qq.com
This work was supported by the State Grid Jibei Electric Power Co., Ltd. Tangshan Power Supply Company (Project No. B3010325Z013).

it difficult to achieve robust detection and accurate pattern identification under varying operating environments [7].

To overcome the limitations of single-modality sensing, multi-sensor and multi-physical-field PD detection methods have attracted increasing attention in recent years. By integrating electrical and non-electrical signals, such as optical, acoustic, or ultrasonic measurements, heterogeneous sensor fusion can significantly enhance detection reliability and spatial localization capability [8-10]. Optical electric-field sensing offers high bandwidth and strong immunity to electromagnetic interference, enabling effective localization of insulation defect regions, while acoustic pressure wave sensing provides complementary information for confirming PD occurrence and discharge intensity. Nevertheless, the effective fusion of heterogeneous signals and the extraction of discriminative features for PD pattern identification remain challenging tasks.

In parallel, data-driven methods based on machine learning and deep learning have been increasingly introduced into PD analysis due to their strong feature learning and pattern recognition capabilities. Traditional machine learning approaches, such as support vector machines [11] and shallow neural networks [12], often rely on handcrafted features and exhibit limited generalization ability. Recent advances in deep learning, particularly convolutional neural networks (CNNs), have demonstrated superior performance in PD classification by automatically learning hierarchical representations from raw data [13,14]. However, directly applying deep learning models to one-dimensional PD time-series signals may fail to fully capture temporal dependencies and global structural characteristics, especially under noisy conditions.

To address this issue, time-series-to-image encoding techniques, such as Gramian Angular Field (GAF) transformation, have been proposed to convert one-dimensional signals into two-dimensional representations, enabling CNN-based models to exploit spatial correlations and topological structures [15-18]. Meanwhile, attention mechanisms have been introduced to further enhance feature discrimination by emphasizing informative channels and suppressing irrelevant information [19-22]. Despite these advances, existing studies often focus on either sensor fusion or deep learning model optimization, while a unified framework that tightly integrates heterogeneous sensing, robust signal processing, and enhanced deep learning for high-voltage cable PD detection and identification is still limited.

Motivated by the above observations, this paper presents a partial discharge detection and identification framework for high-voltage cable systems based on heterogeneous sensor fusion and enhanced deep learning. Optical electric-field and acoustic pressure wave sensors are jointly employed to improve detection reliability and robustness. An improved adaptive-threshold discrete wavelet transform is utilized for signal denoising, followed by an optimized GAF transformation to generate informative two-dimensional feature representations. Furthermore, a residual convolutional neural network incorporating an efficient channel attention mechanism is designed to achieve accurate PD pattern identification. Extensive laboratory experiments and field tests on 220 kV tunnel-laid cable systems are conducted to validate the effectiveness, robustness, and practical applicability of the proposed approach.

The main contributions of this work can be summarized as follows:

1) A heterogeneous sensor fusion-based PD detection framework is developed for high-voltage cable systems, combining optical electric-field and acoustic pressure wave sensing to enhance reliability and anti-interference capability.

2) An integrated signal processing and feature representation scheme is proposed, incorporating adaptive wavelet denoising and optimized GAF transformation to improve feature discriminability.

3) An enhanced deep learning model with residual architecture and channel attention is designed for accurate PD pattern identification, and its effectiveness is verified through comprehensive laboratory and field experiments.

2. System Overall Design

As illustrated in Figure 1, the high-voltage cable partial discharge detection and identification system developed in this study is architected into a three-tier physical structure. The first layer serves as the sensing front-end, primarily composed of high-speed photosensitive electric field sensors and pressure wave sensors. This layer employs non-contact measurement techniques to precisely map the electric field distribution within the cable and acquire raw partial discharge signals. The second layer functions as the data acquisition front-end controller, integrating a low-power main control module, an internal energy storage module, an external power supply interface, a data conversion module, and a data storage module. Its primary responsibility is to act as a bridge for the reliable transmission and analog-to-digital conversion of the partial discharge signals. The third layer constitutes the core computational unit, consisting of a system host pre-installed with proprietary analysis software. This host comprises human-machine interaction (HMI) software, an embedded database of discharge signal characteristics, a cable defect identification system, a data storage module, and a functional management system. It is tasked with the advanced post-processing, recognition, archiving, and management of partial discharge signals, while simultaneously executing supervisory management over the front-end controllers and the sensor array. Figure 2 shows the layout of heterogeneous sensors.

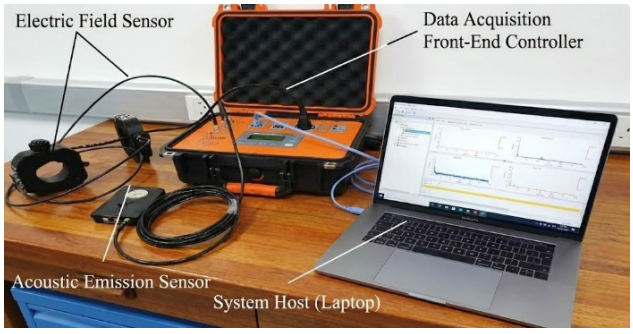

Figure 1. Overall composition and layout of the system

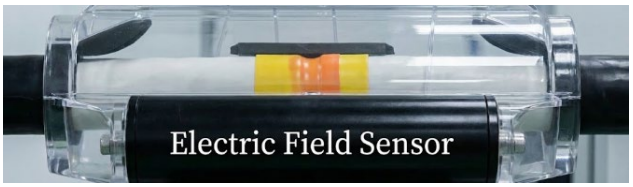

Figure 2. Layout of heterologous sensors

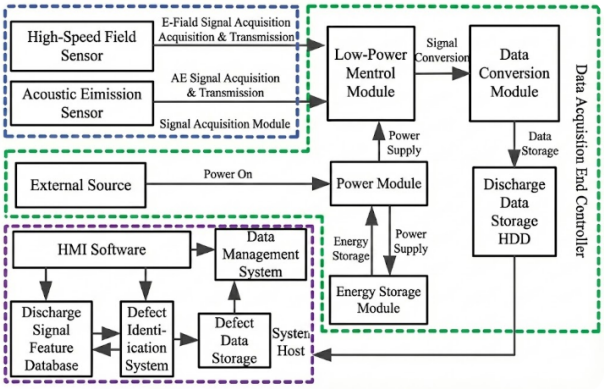

Figure 3. System functional modules and workflow

Figure 3 illustrates the fundamental operational workflow of the proposed system and the interactions among its primary functional modules. The workflow begins with the system host issuing control commands to the heterogeneous sensing units, which consist of an optical electric-field sensor and an acoustic pressure wave sensor. Under the coordinated control of the system host, these sensors continuously monitor the cable under test and synchronously acquire raw time-domain signals corresponding to electric field variations and pressure wave responses induced by partial discharge events.

The acquired raw signals are transmitted to the data acquisition front-end controller through coaxial communication cables and dedicated signal interfaces. At this stage, the front-end controller serves as an intermediary between the heterogeneous sensors and the system host, ensuring signal compatibility and stable data transmission. The front-end controller performs signal conditioning and analog-to-digital conversion to transform the raw analog signals into digital form. The digitized data are temporarily stored in the local storage module of the front-end controller to support buffering and prevent data loss during high-frequency acquisition.

Subsequently, the converted digital signals are transmitted to the system host via an RJ45 Ethernet network interface, enabling reliable and high-speed data communication. Upon receiving the data, the system host carries out comprehensive signal processing, including noise suppression, feature extraction, and pattern analysis. In parallel, the processed data are archived and managed within the system database to facilitate historical data retrieval and long-term condition monitoring.

Finally, the system host integrates the extracted signal features with the embedded discharge characteristic database, which contains representative signatures of different cable fault types. Through feature matching and intelligent inference mechanisms, the system performs diagnosis and identification of specific partial discharge patterns and corresponding cable defects. This closed-loop workflow enables real-time monitoring, accurate fault identification, and effective management of high-voltage cable conditions.

3. System Hardware Scheme

3.1. System Hardware Scheme

Figure 4 illustrates the electric field sensor, which is designed to measure the electric field distribution along the cable without perturbing the original field strength, thereby facilitating the detection of latent insulation hazards. The operation of this sensor is based on the fundamental relationship between electric field strength and electric charge. When a charge moves within an electric field, the force it experiences is directly proportional to the field strength; thus, by measuring the force exerted on the moving charge, the electric field strength can be indirectly derived. This sensor is characterized by high detection precision, enabling the accurate quantification of field variations. It possesses robust immunity to electromagnetic interference and operates non-intrusively, making it suitable for online monitoring. Furthermore, its rapid response speed ensures the timely capture of transient partial discharge events. The primary technical parameters of the electric field sensor are detailed in Table 1.

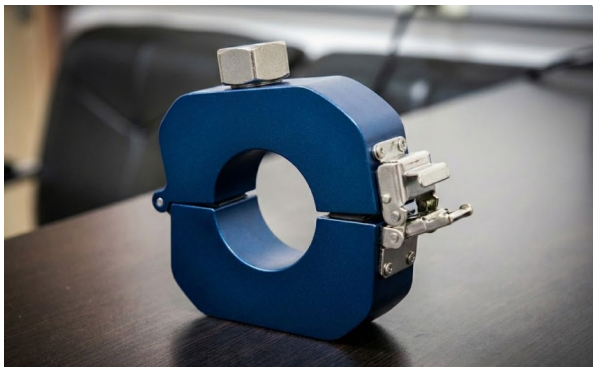

Figure 4. Electric field sensor

Table 1. Main technical parameters of sensors

Parameter	Specification
Voltage Measurement Range / kV	200 ~ 400
Field Strength Measurement Range / kV/cm	2 ~ 10
Input Resistance / MΩ	> 10,00
Input Capacitance / pF	0 < 10
Frequency Response / kHz	7 ~ 100
Measurement Accuracy / %	± 1.5

Figure 5. Pressure wave sensor

Figure 5 presents the pressure wave sensor, which is primarily employed to verify whether partial discharge is occurring in the identified insulation hazard regions. The operating principle of the pressure wave sensor can be described as follows. A pulse signal is injected into the metal shielding enclosure of the unit under test, generating a voltage that is applied to the cable through a limiting resistor. In this configuration, the cable conductor is treated as a high-voltage electrode and serves to provide a driving voltage to the sensor. As a result, the shielding electrode undergoes periodic mechanical vibration, the amplitude of which is proportional to the measured current, enabling the extraction of pressure wave signals associated with partial discharge activity.

To ensure accurate and reliable pressure wave detection, the cable's conductive layer must be tightly coupled with the piezoelectric sensing element via the electrode plate. Proper mechanical contact and impedance matching are essential for efficient signal transmission, as they significantly enhance the sensitivity of the sensor and reduce signal attenuation during pressure wave propagation. This configuration allows the pressure wave sensor to effectively capture mechanical responses induced by partial discharge events, providing complementary non-electrical information for discharge verification.

3.2. Data Acquisition Controller

Figure 6 displays the proprietary data acquisition front-end controller. This integrated unit comprises a low-power main control module, an internal storage module (64GB), dedicated test channels for both electric field and pressure wave signals, an RJ45 Ethernet data interface, a power interface (supporting both 220V AC supply and internal battery operation), a power switch, and status indicator LEDs. The heterogeneous sensors are physically connected to the front-end controller via coaxial communication cables and test channels, enabling signal conversion and local storage. The converted digital signals are subsequently transmitted to the system host via the network interface. The data acquisition controller serves a critical function as a sensor management intermediary. This is necessary because the system host, being a general-purpose computer, typically supports standard digital interfaces (e.g., USB, HDMI), whereas the system sensors utilize specialized digital bus communication protocols. The incompatibility between these protocols prevents direct communication, necessitating the controller to bridge the gap.

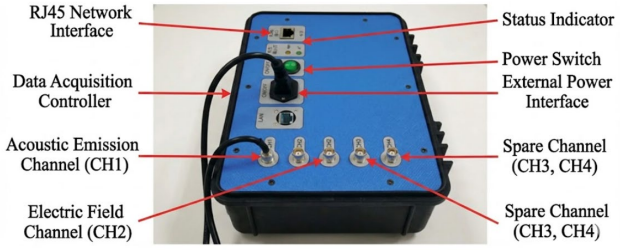

Figure 6. Data acquisition front-end controller

3.3. System Host

Figure 7 depicts the system host, which is installed with the partial discharge signal analysis and identification system. It is equipped with capabilities for signal noise suppression, key feature extraction, inference mechanisms, and expert diagnostics. The inference mechanism functions by evaluating the key characteristic parameters of the discharge signal; if these parameters exceed pre-set thresholds, the inference rules are activated to issue a preliminary warning of cable defects. The expert diagnosis function utilizes an improved adaptive threshold wavelet transform to decompose the defect characteristics of the tested cable into different time and frequency domains, enabling the location of effective distortion points at any level of detail. By leveraging an improved Residual Convolutional Neural Network (ResNet) in conjunction with the system's embedded partial discharge feature database, the host performs data comparison to identify the specific type of cable partial discharge. Additionally, the system host provides functionalities for data

storage and playback, as well as database and sensor management.

Figure 7. Host for installing signal analysis and recognition system

4. System Detection Mechanism and Method

Based on the detection principles of electric fields and pressure waves associated with cable partial discharge (PD), the raw signals acquired by the heterogeneous sensors are transmitted to the system host. Upon reception, the system executes a comprehensive analysis sequence on the input signals. As illustrated in Figure 8, this process comprises three critical stages: raw signal noise suppression, signal feature transformation, and discharge pattern (or cable defect) identification.

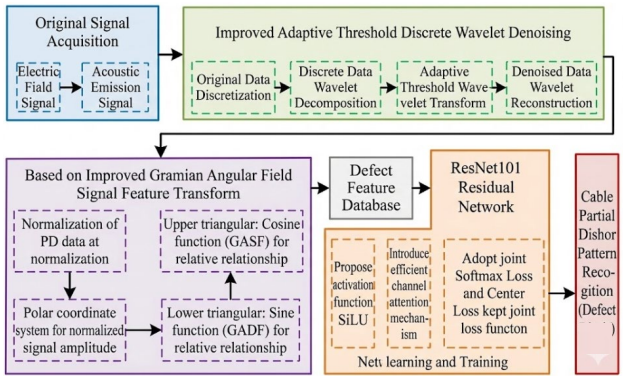

Figure 8. Process of cable partial discharge pattern recognition

4.1. Detection Mechanism

To guarantee the reliability of the detection process, the system employs a fusion of electric field and pressure wave sensors to monitor partial discharge phenomena. The detection protocol initiates with the electric field sensor performing real-time monitoring of the internal electric field distribution of the cable. This allows for the localization of potential insulation hazard areas and the recording of electrical signals generated by partial discharge, constituting the primary detection phase. Subsequently, the pressure wave sensor is utilized to verify whether a pressure wave has been generated in the identified hazard zone, thereby confirming the occurrence of partial discharge and recording the associated non-electrical signals, which constitutes the secondary detection phase. The overall system detection mechanism is depicted in Figure 9.

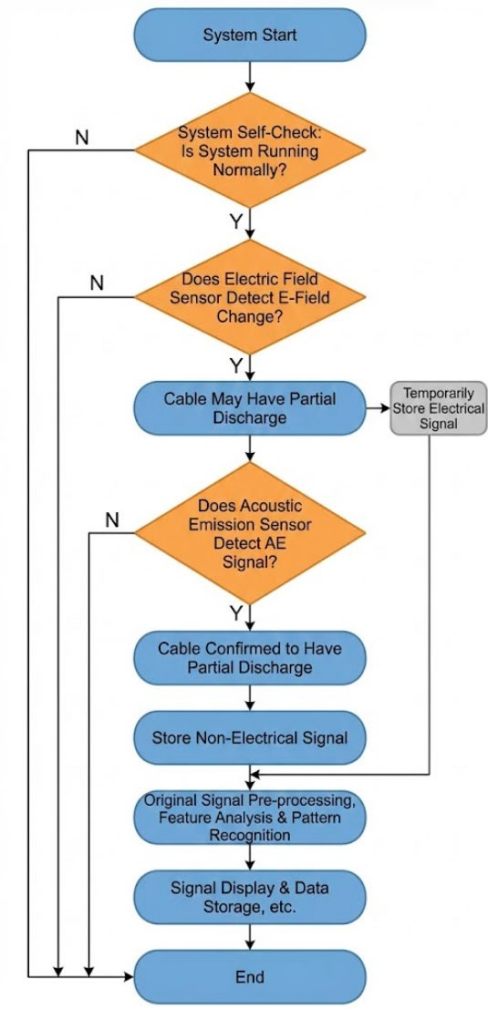

Figure 9. Detection and recognition mechanism

Focusing on the pressure wave detection principle, the phenomenon is elucidated using air gap discharge as a paradigm. When partial discharge occurs, the air gap undergoes periodic expansion and compression, exerting reciprocating extrusion and tension on the cable dielectric. This results in a periodic vibration signal. Since the frequency of the pressure wave generated by this vibration is typically high and its wavelength is far greater than the dimensions of

the air gap, the oscillatory mechanical process at the air gap can be analogized to the zero-input response of a second-order circuit, yielding:

$$f_n C_m \frac{d^2 u_c}{dt^2} + R_n C_m \frac{du_c}{dt} + u_c = 0 \quad (1)$$

where M_m, C_m, and R_m represent mass, compliance, and mechanical resistance, respectively; t is the discharge time; and u_c is the external force exerted by the air gap wall.

The periodic expansion and compression of the air gap induce pressure variations that form the pressure wave. The external force of the air gap wall (i.e., pressure) divided by the surface area of the air gap yields the pressure intensity of the wave generated by the partial discharge. Consequently, the pressure intensity is directly proportional to the external force of the air gap wall, and their variation frequencies are identical. Therefore, solving for the external force is essential. Deriving from (1), the external force of the air gap wall is expressed as:

$$u_c = \frac{U_0 \omega_0}{\omega} e^{\frac{R_m t}{2M_m}} sin(\omega t + \arctan \frac{2M_m \omega}{R_m}) \quad (2)$$

where ω is the angular frequency of the pressure wave signal, and U_0 represents the initial force on the air gap surface. These are defined as:

$$\begin{cases} \omega = \sqrt{\frac{1}{M_m C_m} - (\frac{R_m}{M_m})^2} \\ \omega_0 = \sqrt{(\frac{R_m}{2M_m})^2 + \omega^2} \\ U_0 = QE \end{cases} \quad (3)$$

where Q is the discharge magnitude of the air gap, and E is the breakdown field strength.

4.2. Signal Denoising Method

Given the complexity of cable engineering environments, the raw partial discharge signals acquired by the system inevitably contain noise. To enable rapid and accurate diagnosis of cable partial discharge faults, this study employs an improved adaptive threshold discrete wavelet transform (DWT) for signal pre-processing. The fundamental workflow, as shown in Figure 10, involves four distinct steps: discretization of raw data, wavelet decomposition of discrete data, wavelet transformation based on adaptive thresholds, and wavelet reconstruction of the denoised data.

Mathematically, assuming a mother wavelet signal $\varphi(t)$ exists in the real number space $L^2(R)$, its Fourier transform $\Psi(\omega)$ must satisfy the wavelet admissibility condition:

$$\int_{-\infty}^{+\infty} \frac{|\Psi(\omega)|^2}{\omega} d\omega < \infty \quad (4)$$

Subsequently, the wavelet basis function $\Phi_{a,b}(t)$ is obtained and expressed as:

$$\varphi_{a,b}(t) = \frac{\varphi(\frac{t-b}{a})}{\sqrt{a}} \quad (5)$$

where a is the scaling (dilation) factor with $a > 0$, and b is the translation factor. To perform the discrete transform, the scaling factor a and translation factor b are discretized as follows:

$$\begin{cases} a = a_0^m, a_0 > 0, m \in Z \\ b = n b_0 a_0^m, b_0 > 0, n \in Z \end{cases} \quad (6)$$

Substituting (6) into (5) yields the discrete wavelet basis function $\varphi_{m,n}(t)$, expressed as:

$$\varphi_{m,n}(t) = \varphi(\frac{t - n b_0 a_0^m}{a_0^m}) / a_0^{\frac{m}{2}} \quad (7)$$

Defining $\overline{\varphi}(t)$ as the conjugate of $\varphi(t)$, for a raw partial discharge signal $x(t) \in L^2(R)$, the discrete wavelet transform $WT_x(m,n)$ is obtained as:

$$WT_x(m,n) = \int_{-\infty}^{+\infty} x(t) \overline{\varphi}_{m,n}(t) dt = \langle x(t), \varphi_{m,n}(t) \rangle \quad (8)$$

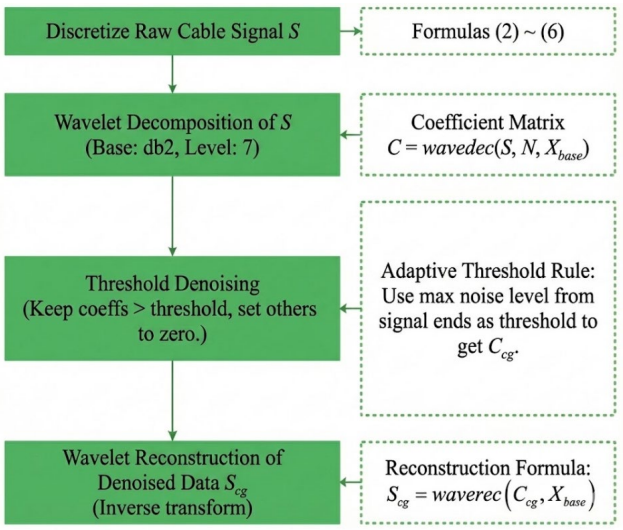

Figure 10. Discrete wavelet denoising based on adaptive threshold

4.3. Signal Feature Transformation via GAF

To enhance data classification features and facilitate subsequent image recognition training, an improved Gramian Angular Field (GAF) feature transformation method is proposed. This method converts the one-dimensional time-series signal of cable partial discharge into a two-dimensional topological feature image. The specific process is as follows.

First, the partial discharge data at each time point is normalized:

$$\overline{v}_i(t) = \frac{v_i(t) - v_{min}}{v_{max} - v_{min}} \quad (9)$$

where $\overline{v}_i(t)$ is the normalized signal amplitude at time node i; $v_i(t)$ is the original amplitude; and v_{max} and v_{min} are the maximum and minimum values of the signal, respectively.

Next, the normalized signal amplitude data is represented in a polar coordinate system:

$$\begin{cases} \phi_i(t) = \arccos[\overline{v}_i(t)] \\ \phi_i(t) \in [0, \pi/2] \\ r_i = i/N, i = 1,2,\ldots,N \end{cases} \quad (10)$$

where $\phi_i(t)$ and r_i represent the angle and radius corresponding to $\overline{v}_i(t)$ in the polar coordinate system, and N is the number of nodes.

Finally, a trigonometric transformation is performed on the amplitude data of different nodes in the polar system:

$$G = [\overline{v}_i(t) \oplus \overline{v}_j(t)]_{i,j=1}^{N} \quad (11)$$

Using the cosine of the sum of two angles calculates the Gramian Angular Sum Field (GASF), while using the sine of the sum calculates the Gramian Angular Difference Field (GADF). To better characterize the topological information within the partial discharge time-series signal and enhance the distinguishability of different defects, this study proposes an improved GAF transformation that considers the monotonic characteristics of the Sum and Difference fields in different intervals. Specifically, the cosine function (GASF) is used to represent the relative relationships in the upper triangular elements, while the sine function (GADF) represents the lower triangular elements, as expressed below:

$$\overline{v}_i(t) \oplus \overline{v}_j(t) = \begin{cases} \cos[\phi_i(t) + \phi_j(t)], i \le j \\ \sin[\phi_i(t) - \phi_j(t)], i > j \end{cases} \quad (12)$$

Using this improved Gramian Angular Field feature transformation, 1D time-series signals of spike discharge, air gap discharge, and surface discharge are converted into 2D topological feature images, as shown in Figure 11.

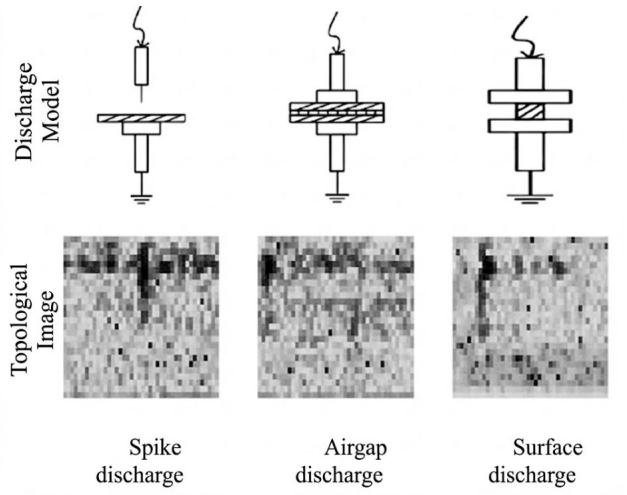

Figure 11. Partial discharge model and topological image

4.4. Enhanced Deep Learning Model Design

Residual Neural Networks (ResNet) facilitate training by adding shortcut connections and introducing residuals and identity mapping, thereby avoiding the gradient vanishing or explosion problems common in traditional CNNs. The ResNet101 network is particularly adept at learning complex features from input data, making it highly suitable for image recognition tasks where accuracy is paramount. Considering network complexity, computational load, and feature extraction capability, this study adopts the ResNet101 model for partial discharge pattern recognition, implementing improvements in three key areas: the activation function, the residual module, and the loss function, as illustrated in Figure 12.

Regarding the practical deployment of the model, the improved ResNet101 architecture, while ensuring high recognition accuracy, has relatively high computational complexity and memory usage, which limits direct deployment on edge devices with limited computing power for real-time monitoring. However, balancing performance and efficiency is feasible through targeted network simplification: first, retain core components that determine recognition accuracy, including optimized GAF feature transformation, ECA attention mechanism, and the combined Softmax-Center loss function; second, adopt lightweight optimization strategies such as replacing the ResNet101 backbone with lightweight networks to reduce the number of convolutional layers and parameters, and apply network pruning and 8-bit quantization techniques to further reduce computational load and storage space without significant loss of feature expression. Preliminary simulation results show that after simplification, the model's computational load can be reduced by more than 50%, inference speed increased by 2-3 times, and recognition accuracy loss controlled within 3%. Future work will conduct systematic experiments on model simplification, verify the performance-efficiency balance on mainstream edge computing platforms, and develop a lightweight model suitable for edge deployment to realize real-time online monitoring of high-voltage cables in distributed scenarios.

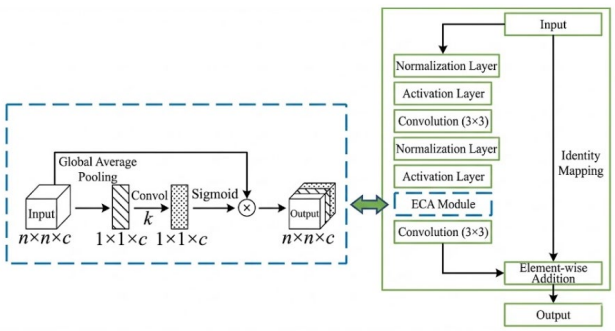

Figure 12. Residual unit integrating efficient channel attention mechanism

Activation Function Improvement

Building upon the traditional ReLU activation function, the SiLU (Sigmoid Linear Unit) activation function is proposed for the base network model. The calculation for the SiLU function f_{SiLU} and its first derivative f'_{SiLU} is:

$$\begin{cases} f_{SiLU} = x \cdot \sigma(x) \\ f'_{SiLU} = f_{SiLU} + \sigma(x)(1 - f_{SiLU}) \\ \sigma(x) = \dfrac{1}{1+e^{-x}} \end{cases} \quad (13)$$

where x is the input from the upper layer node, and $\sigma(x)$ is the Sigmoid function. The curve of the f_{SiLU} function is smooth and non-monotonic, which enhances the overall performance of the neural network. In the curve of the first derivative f'_{SiLU}, the global minimum where the derivative is 0 acts as a regulator on weights, suppressing the update of large weights and effectively preventing gradient explosion or disappearance.

Residual Module Improvement

While residual blocks mitigate gradient dispersion, feature extraction is still affected by factors such as low contrast and complex textures in topological images. Therefore, this study introduces an Efficient Channel Attention (ECA) mechanism before the final convolution of the residual unit. The principle involves adaptively calibrating responses between different channels to learn the importance of each feature channel and enhance the feature weights beneficial for defect classification. The process includes: global average pooling to compress the input feature map size; 1D convolution (kernel size k) to realize local cross-channel interaction; and using a Sigmoid function to obtain channel weights. The kernel size k is determined by:

$$k = \left| \frac{\log_2(C)}{\gamma} + \frac{b}{2} \right|_{odd} \quad (14)$$

where $|\cdot|_{odd}$ indicates the nearest odd number; C is the number of channels; and γ and b are parameters.

Loss Function Improvement

Since partial discharge signals from different cable defects can be similar, the standard Softmax loss function L_S of ResNet101 is insufficient for precise classification. Considering that the Center Loss function L_C effectively increases inter-class feature spacing, this study integrates L_C into the network's loss layer. The combined loss function L, designed to enhance the model's ability to classify different defects, is calculated as:

$$\begin{aligned} L &= L_S + \lambda L_C \\ &= -\sum_{k=1}^{M} \log \frac{e^{W_{y_k}^T x_k + b_{y_k}}}{\sum_{j=1}^{N} e^{W_j^T x_k + b_j}} + \frac{\lambda}{2} \sum_{k=1}^{M} || x_k - c_{y_k} ||_2^2 \end{aligned} \quad (15)$$

where λ is the weight balancing the two loss functions (set to 0.2); x_k is the classification feature learned before the fully connected layer; W is the output of the fully connected layer; M is the training batch size; N is the number of defect categories; and c_{y_k} is the feature center of the y_k-th defect.

5. System Detection Mechanism and Method

To validate the operational performance of the self-developed system, comprehensive performance tests were conducted in both laboratory settings and actual engineering environments. Common cable insulation defects—specifically spike discharge, air gap discharge (internal discharge), and surface discharge—were selected as the primary subjects of study. The system was utilized to acquire various characteristic representations of PD, including time-domain waveforms, discharge rate spectra, Phase Resolved Partial Discharge (PRPD) patterns, Phase Resolved Pulse Sequence (PRPS) patterns, and elliptic diagrams. Subsequently, the signal characteristics were analyzed, and the cable discharge modes were identified by cross-referencing the signal feature database.

5.1. Laboratory Characterization of Discharge Patterns

Figure 13 presents the multi-view characterization of cable shell spike discharge captured by the system, including the discharge rate spectrum, PRPD pattern, PRPS pattern, and elliptic diagram.

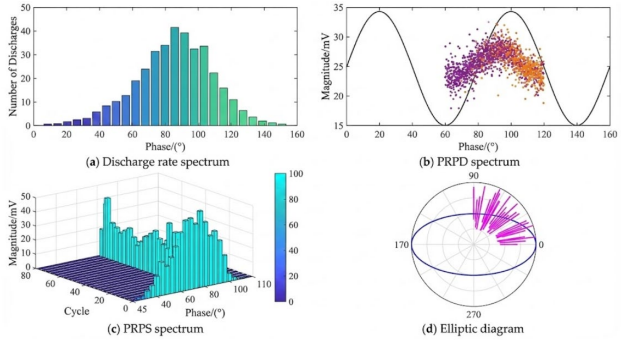

Figure 13. Multi-view characterization of spike discharge characteristics

It is observed that the spike discharge occurrences are predominantly concentrated in the phase interval of $60^\circ \sim 90^\circ$. The distribution exhibits a characteristic pattern where discharge frequency is dense in the center and sparse at the edges, with discharge amplitudes approximating 15 mV.

Analysis indicates that significant burrs or protrusions on the surface of the cable shell induce a non-uniform electric field distribution. This leads to a substantial accumulation of

charge around the protrusion, which continuously impacts the insulating cable, ultimately triggering partial discharge. Consequently, it is imperative to improve material selection and manufacturing processes, and to strictly adhere to protocols for polishing burrs to mitigate discharge caused by surface irregularities.

Air gap discharge primarily refers to partial discharge occurring within voids or cavities in the cable insulation layer. Figure 14 displays the discharge rate spectrum, PRPD pattern, PRPS pattern, and elliptic diagram for cable air gap discharge acquired by the system.

The data reveals that air gap discharge occurrences are concentrated in the phase intervals of $0^{\circ} \sim 90^{\circ}$ and $180^{\circ} \sim 270^{\circ}$, with discharge amplitudes hovering around 20 mV.

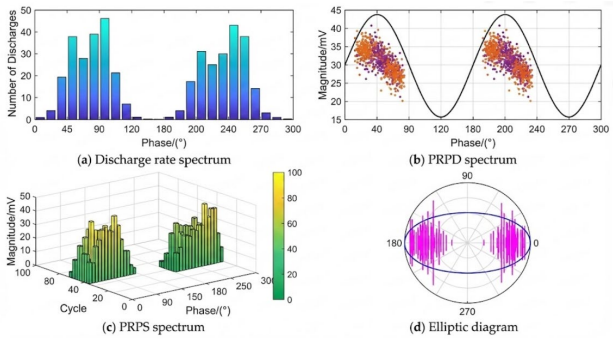

Figure 14. Multi-view characterization of air gap discharge characteristics

Table 2. Testing data of pattern recognition

Trial Number	Actual Discharge	Self-developed Identification	Self-developed Accuracy	Third-party Identification	Third-party Accuracy
1	Point Discharge	Point Discharge	Yes	Point Discharge	Yes
2	Air Gap Discharge	Air Gap Discharge	Yes	Air Gap Discharge	Yes
3	Point Discharge	Point Discharge	Yes	Point Discharge	Yes
4	Surface Discharge	Surface Discharge	Yes	Surface Discharge	Yes
5	Air Gap Discharge	Point Discharge	No	Missed Detection	No
6	Surface Discharge	Surface Discharge	Yes	Surface Discharge	Yes
7	Point Discharge	Point Discharge	Yes	Point Discharge	Yes
8	Surface Discharge	Surface Discharge	Yes	Surface Discharge	Yes
9	Surface Discharge	Surface Discharge	Yes	Surface Discharge	Yes
10	Point Discharge	Point Discharge	Yes	Point Discharge	Yes
11	Air Gap Discharge	Point Discharge	No	Air Gap Discharge	Yes
12	Air Gap Discharge	Air Gap Discharge	Yes	Air Gap Discharge	Yes
13	Surface Discharge	Surface Discharge	Yes	Surface Discharge	Yes
14	Point Discharge	Point Discharge	Yes	Point Discharge	Yes
15	Point Discharge	Point Discharge	Yes	Air Gap Discharge	No
16	Surface Discharge	Surface Discharge	Yes	Surface Discharge	Yes
17	Air Gap Discharge	Air Gap Discharge	Yes	Air Gap Discharge	Yes
18	Surface Discharge	Surface Discharge	Yes	Surface Discharge	Yes

19	Surface Discharge	Surface Discharge	Yes	Surface Discharge	Yes
20	Air Gap Discharge	Air Gap Discharge	Yes	Air Gap Discharge	Yes
21	Point Discharge	Point Discharge	Yes	Point Discharge	Yes
22	Point Discharge	Point Discharge	Yes	Point Discharge	Yes
23	Surface Discharge	Surface Discharge	Yes	Air Gap Discharge	No
24	Air Gap Discharge	Air Gap Discharge	Yes	Air Gap Discharge	Yes
25	Air Gap Discharge	Air Gap Discharge	Yes	Air Gap Discharge	Yes
Performance Analysis		Detection Rate: (25/25) 100%	Recognition Rate: (24/25) 96.0%	Detection Rate: (24/25) 96.0%	Recognition Rate: (23/25) 92.0%

Table 3. Comparative analysis of cable discharge pattern recognition results in engineering applications

Identification Number	Actual Situation	Self-developed System Identification Result	Third-party System Identification Result
16	No Discharge	No Discharge	Point Discharge
41	No Discharge	No Discharge	Missed Detection/No Data
43	No Discharge	No Discharge	Air Gap Discharge
77	No Discharge	No Discharge	Missed Detection/No Data
121	No Discharge	No Discharge	Missed Detection/No Data
Identification Number	Actual Situation	Self-developed System Identification Result	Third-party System Identification Result

Under the influence of high voltage, partial discharge caused by such cable defects can be severe, easily leading to breakdown phenomena. Furthermore, the morphology, size of the air gap, and the properties of the gas within the void significantly influence the partial discharge breakdown effects in the cable insulation.

5.2. Partial Discharge Detection and Recognition Performance Analysis

The ultimate objective of this study is to achieve online status monitoring for live high-voltage cables. Therefore, it is essential to evaluate the discharge recognition performance of the self-developed system. To benchmark its capabilities, a commercially available third-party detection system (with its fault feature database capacity modified to match the self-developed system for fair comparison) was introduced under identical test parameters and environmental conditions.

Sixty random partial discharge tests were conducted. Table 2 lists data from 25 arbitrarily selected test instances.

As shown in Table 2, the discharge detection rate (the ratio of detected PD events to actual PD events) of the self-developed system was 100%, surpassing the 96.0% rate of the third-party system. The cable defect recognition rate (the ratio of accurately identified discharge types to actual PD events) was 96.0%, which is also superior to the 92.0% recognition rate of the third-party system. These results demonstrate the robust pattern recognition capabilities of the self-developed system and verify its superior detection performance in a controlled environment.

It should be noted that the current laboratory tests focus on single-defect scenarios, and systematic verification for multi-defect coexistence scenarios is not yet conducted. From the model's design mechanism, the proposed framework has inherent adaptability potential for multi-defect scenarios: the optimized GAF transformation can integrate mixed discharge time-series signals into comprehensive topological feature images, and the ECA attention mechanism in the improved ResNet101 can adaptively calibrate feature weights of different defects to distinguish overlapping characteristic information. However, the interaction between multiple defects may cause signal distortion or overlap, which may theoretically lead to a slight decrease in recognition accuracy, but there is no evidence of a significant drop. Future research will construct a multi-defect coexistence experimental platform, simulate common combined defect types, expand the defect feature database with mixed discharge samples, and optimize the model's feature fusion strategy to further verify and improve recognition accuracy under multi-defect coexistence.

5.3. Engineering Application Verification

To further validate the practical performance of the system in engineering scenarios, the self-developed high-voltage cable

PD detection and identification system was deployed for the inspection of a 220kV tunnel cable network, commissioned by the Electric Power Research Institute (EPRI) of a municipality directly under the central government.

During the inspection, field personnel operated the third-party detection system currently used by the EPRI alongside the self-developed system (which utilized a defect feature database matched in capacity to the third-party system, though more refined than in the lab tests). Both systems executed 122 simultaneous detection tests in the same environment. Partial results are shown in Table 3.

The third-party system exhibited a discharge detection rate of 97.54% and a pattern recognition rate of 95.90%, indicating some false positives or data gaps. In contrast, the self-developed system did not detect any partial discharge phenomena, concluding "No Discharge." This conclusion was fully consistent with the actual on-site conditions (the tunnel cable line was indeed free of defects), yielding a 100% rate for both detection and pattern recognition. A comparison of experimental and engineering test cases reveals that as the fault characteristic database becomes more comprehensive, the performance improvement (or self-learning capability) of the self-developed system outpaces that of the third-party system. Currently, the system has passed testing by a CNAS-accredited third-party qualification agency and has been delivered to the EPRI for technical acceptance.

It is worth emphasizing that the field tests were conducted in a 220 kV tunnel environment with relatively stable temperature, humidity, and cleanliness. In practical engineering, high-voltage cables may face extreme conditions such as extreme temperature (-40°C ~ 60°C), high humidity (relative humidity > 95%), and severe pollution (surface dust accumulation, chemical corrosion), which require further enhancement of sensor stability and model robustness. For sensors: extreme temperature may affect the response speed of the optical electric-field sensor's photosensitive components and the piezoelectric effect of the pressure wave sensor, while high humidity and pollution may cause insulation degradation of the sensor's external packaging and signal attenuation. Future optimization will focus on adding temperature compensation modules and waterproof/dustproof protective casings to improve environmental adaptability. For the model: the existing training dataset lacks samples collected under extreme environments, which may lead to performance degradation when facing unseen extreme environmental noise. Subsequent work will collect discharge signals under extreme conditions, construct a cross-environment dataset, and introduce domain adaptation algorithms (e.g., domain-adversarial training) to enhance the model's generalization ability, ensuring high detection and recognition accuracy under harsh conditions.

6. Conclusion

This study has successfully designed and implemented a high-voltage cable partial discharge (PD) detection and identification system, validated through both rigorous laboratory testing and practical engineering deployment. The core contributions and conclusions are as follows:

1) By integrating high-speed optical electric field sensors with pressure wave sensors, the system establishes a non-intrusive, "electrical plus non-electrical" dual-sensing framework. This approach effectively isolates partial discharge signals from environmental noise, solving the interference challenges inherent in traditional single-source detection methods.

2) The system employs a sophisticated algorithmic pipeline, utilizing adaptive threshold wavelet transforms for signal denoising and GAF to convert 1D signals into topological features. Furthermore, the integration of an improved ResNet101 model—enhanced with ECA mechanisms and a joint Loss function—enables the precise classification of complex discharge patterns, such as spike, air gap, and surface discharges.

3) Experimental results confirm the system's high reliability, achieving a 100% detection rate and 96.0% recognition accuracy in laboratory environments. In a comparative field application within a 220kV cable tunnel, the system demonstrated superior stability over existing third-party solutions. Notably, the system exhibits a "self-learning" capability, where the continuous enrichment of its fault feature database progressively enhances recognition precision in real-world scenarios.

The discussions on multi-defect coexistence recognition, extreme environment adaptability, and edge device deployment provide important directions for the further improvement and practical promotion of the system. By continuously optimizing the experimental design, enriching the dataset, and improving the model structure, the system's applicability and reliability in complex practical scenarios will be further enhanced, providing more comprehensive technical support for the condition monitoring of high-voltage cable systems.

References

[1] Wang S, Liu J, Li Z, et al. Diagnosis and location of defects in a cross-bonding cable system based on multi-phase high-voltage high-frequency collaborative excitation[J]. IEEE Transactions on Industrial Electronics, 2024, 71(11): 14946-14956.

[2] Elsaid A M, Zahran M S, Abdel Moneim S A, et al. A recent review on ventilation and cooling of underground high-voltage cable tunnels[J]. Journal of Thermal Analysis and Calorimetry, 2024, 149(17): 8927-8978.

[3] Yang S, Pang X, Zhang P, et al. A distributed PD detection method for high voltage cables based on high precision clock synchronization[J]. Measurement, 2025, 241: 115731.

[4] Liu H, Li H, He N, et al. Design of an Ultra-High-Frequency Through-Core Current Transformer for Cable Partial Discharge Detection[J]. Electronics, 2025, 14(13): 2547.
[5] Li A, Wei G, Li S, et al. Pattern recognition of partial discharge in high-voltage cables using TFMT model[J]. IEEE Transactions on Power Delivery, 2024.
[6] Wang H, Xiao G, Wang L, et al. High-frequency current transformer design and analysis for partial discharge detection of power electronic modules[J]. IEEE Transactions on Power Electronics, 2025.
[7] Robles G, Martínez-Tarifa J M, Barroso-de-María G, et al. High-Frequency Current Transformer Design to Detect Serial Arcs in More Electric Aircraft[J]. IEEE Transactions on Transportation Electrification, 2024, 11(1): 639-647.
[8] Liu Z, Wu W, Li J, et al. Research on Intelligent Diagnosis Method for High Voltage Cable Insulation Faults Based on Multi-Sensory Fusion[C]//2024 The 9th International Conference on Power and Renewable Energy (ICPRE). IEEE, 2024: 102-107.
[9] Xu C, Wu X, Fang J, et al. Multi-sensor multi-dimensional data fusion method for submarine cable anchor damage event identification[J]. Ocean Engineering, 2025, 341: 122458.
[10] Zhong L, Liang K, Liu H, et al. Diagnosis Method for Ablation Defects in High-Voltage Cable Buffer Layers Based on an Artificial Olfactory System[J]. IEEE Sensors Journal, 2025.
[11] Luo D, Yao N, Zhang Y, et al. Partial Discharge Detection of High Voltage Electrical Equipment using Multiclass Support Vector Machine[C]//2024 First International Conference on Software, Systems and Information Technology (SSITCON). IEEE, 2024: 1-5.
[12] Saad M H, Hashima S, Omar A I, et al. Deep learning approach for cable partial discharge pattern identification[J]. Electrical Engineering, 2025, 107(2): 1525-1540.
[13] Sun C, Wu G, Pan G, et al. Convolutional neural network-based pattern recognition of partial discharge in high-speed electric-multiple-unit cable termination[J]. Sensors, 2024, 24(8): 2660.
[14] Zhang Z, Wu H, Ren W, et al. Research on Partial Discharge Spectrum Recognition Technology Used in Power Cables Based on Convolutional Neural Networks[J]. Inventions, 2025, 10(2): 25.
[15] Sun C, Wu G, Xin D, et al. Defect identification method of cable termination based on improved gramian angular field and resnet[J]. Recent Advances in Electrical & Electronic Engineering (Formerly Recent Patents on Electrical & Electronic Engineering), 2024, 17(2): 159-169.
[16] Kumar H, Shafiq M, Kauhaniemi K, et al. A review on the classification of partial discharges in medium-voltage cables: detection, feature extraction, artificial intelligence-based classification, and optimization techniques[J]. Energies, 2024, 17(5): 1142.
[17] Zhu G, Wang S, Zhang Y, et al. Partial Discharge Pattern Recognition in High Voltage Transmission Cable Project[C]//2024 IEEE 4th International Conference on Electronic Technology, Communication and Information (ICETCI). IEEE, 2024: 1170-1173.
[18] Chang C K, Boyanapalli B K. Study of partial discharges measurement cycles effect on defect recognition for underground cable joints[J]. Measurement Science and Technology, 2024, 35(6): 065406.
[19] Wu G, Zhang T, Cao B, et al. A review and progress of insulation fault diagnosis for cable using partial discharge approach[J]. IEEE Transactions on Dielectrics and Electrical Insulation, 2024.
[20] Liu C, Qi Y, Zhang Y, et al. Diagnosis Method for Partial Discharge Faults in Power Cables Based on Deep Learning[C]//2024 The 9th International Conference on Power and Renewable Energy (ICPRE). IEEE, 2024: 91-96.
[21] Chen L, Li Q, Long G, et al. Cable partial discharge identification network based on adaptive residual diffusion denoising and morphological attention[J]. Scientific Reports, 2025, 15(1): 42848.
[22] Roy S S, Paramane A, Singh J, et al. Image Visibility Patch-Aided Partial Discharge Recognition Framework for Identifying Defects in XLPE Cables[J]. IEEE Transactions on Instrumentation and Measurement, 2025.